RESEARCH

Histological, functional and transcriptomic alterations in the juvenile hippocampus in a mouse model of thyroid hormone resistance

Yingxin Fang[1,*], Pingping Dang[1,*], Yue Liang[1], Defa Zhao[1], Ranran Wang[1], Yue Xi[1,2], Dan Zhang[1,2], Wei Wang[1], Zhongyan Shan[1], Weiping Teng[1] and Xiaochun Teng[1]

[1]Department of Endocrinology and Metabolism, Institute of Endocrine, NHC Key Laboratory of Diagnosis and Treatment of Thyroid Diseases, The First Hospital of China Medical University, Shenyang, People's Republic of China
[2]Department of Endocrinology and Metabolism, The Third Affiliated Hospital of Jinzhou Medical University, Jinzhou, People's Republic of China

Correspondence should be addressed to X Teng: tengxiaochun@126.com

*(Y Fang and P Dang contributed equally to this work)

Abstract

Background: Proper thyroid hormone signaling via the TRα1 nuclear receptor is required for normal neurodevelopmental processes. The specific downstream mechanisms mediated by TRα1 that impact brain development remain to be investigated.
Methods: In this study, the structure, function and transcriptome of hippocampal tissue in a mouse model expressing the first RTHα mutation discovered in a patient, *THRA*^{E403X}, were analyzed. RNAscope was used to visualize the spatial and temporal expression of *Thra1* mRNA in the hippocampus of WT mice, which is corresponding to *THRA1* mRNA in humans. The morphological structure was analyzed by Nissl staining, and the synaptic transmission was analyzed on the basis of long-term potentiation. The Morris water maze test and the zero maze test were used to evaluate the behavior. RNA-seq and quantitative real-time PCR were used to analyze the differentially expressed genes (DEGs) of the hippocampal tissues in the mouse model expressing the *Thra*^{E403X} mutation.
Results: The juvenile mutant *Thra*^{E403X} mice presented with delayed neuronal migration, disordered neuronal distribution, and decreased synaptic plasticity. A total of 754 DEGs, including 361 upregulated genes and 393 downregulated genes, were identified by RNA-seq. DEG-enriched Gene Ontology (GO) and KEGG pathways were associated with PI3K-Akt signaling, ECM–receptor interaction, neuroactive ligand–receptor interaction, and a range of immune-related pathways. 25 DEGs were validated by qPCR.
Conclusions: The *Thra*^{E403X} mutation results in histological and functional abnormalities, as well as transcriptomic alterations in the juvenile mouse hippocampus. This study of the *Thra*^{E403X} mutant offers new insights into the biological cause of RTHα-associated neurological diseases.

Key Words

- thyroid hormone resistance
- hypothyroidism
- hippocampus
- cognitive deficits

https://etj.bioscientifica.com
https://doi.org/10.1530/ETJ-21-0097

Introduction

Thyroid hormones (THs, namely, the prohormone thyroxine T4 and its active form, triiodothyronine T3) play pivotal roles in diverse aspects of life, mainly during development, when they regulate skeletal growth, cardiac function, metabolism, and the nervous system (1, 2, 3). T3 acts predominantly by binding to thyroid hormone receptors (TRα and TRβ), which are encoded by two separate genes, *THRA* and *THRB* in humans and *Thra* and *Thrb* in mice (4).

Resistance to thyroid hormone α (RTHα) is a rare genetic disease caused by mutations in the *THRA* gene that was first described in 2012 (5). Using whole-exome sequencing, the patient was found to be carrying a heterozygous *de novo* mutation (c1207G→T, p.E403X) in *THRA* and presented intellectual disability in childhood that resembles congenital hypothyroidism (6). Although treatment with THs leads to improvements in certain clinical phenotypes of patients with RTHα, including constipation and problems with nerve conduction, the cognitive deficits typically remain (7). Mounting evidence suggests that as one of the most extensively investigated regions in the brain, the hippocampus mediates cognitive functions, notably, learning, and memory functions. In both animals and humans, the hippocampus is vulnerable to hypothyroidism, regardless of the time it begins or its duration (8, 9, 10).

We generated a novel knock-in mouse model ($Thra^{E403X}$) with a phenotype that corresponds to that of the nonsense mutation derived from a patient with RTHα. Specifically, the mutant mice presented features of the $THRA^{E403X/+}$ phenotype, including neurological and motor coordination deficits (11). Unfortunately, the mechanism by which RTHα causes these neurocognitive deficits has not been adequately characterized.

Here, we analyzed the spatiotemporal expression of *Thra*1 mRNA in the hippocampus of mouse and identified hippocampal morphological alterations manifesting in juvenile mice. Furthermore, we employed RNA-seq technology and bioinformatics analysis to identify dysregulated genes that may be associated with the $Thra^{E403X}$ mutation. Finally, 25 candidate DEGs were selected for qPCR analysis. These findings represent an essential starting point for the comprehension of crucial molecules and mechanisms of cognitive deficiency caused by RTHα, especially during the early stage of the disease.

Materials and methods

Animal maintenance

$Thra^{E403X}$ mutant mice, and WT littermates were used in the present study. The $Thra^{E403X}$ mouse strain carries the dominant negative E403X mutation in the *Thra* gene, which has been described previously (11). The mice were housed at 22 ± 2°C for 12 h light:12 h darkness cycle with *ad libitum* access to water and rodent chow. $Thra^{E403X}$ mutant mice and WT mice were obtained by crossing heterozygous mutant mice. Animals were tagged and randomly allocated to each group. All animal care and experimental procedures were approved by the Animal Care and Use Committee at China Medical University.

In situ hybridization

RNAscope, a new ultrasensitive *in situ* hybridization method (12), was used to detect *Thra1* mRNAs (NM_178060.4) in the hippocampus of mouse. The probes for *Thra1* (nine synthetic oligonucleotides complementary to the nucleotide sequence 1836–2336 of *Thra1*) were provided by Advanced Cell Diagnostics (#531731, ACD, San Francisco, CA, USA), which only detect *Thra1* and do not cross detect *Thra2*. The probes for the positive and negative controls were designed to detect the mouse housekeeping gene *Ppib* (#313911, ACD) and the bacterial gene *DapB* (#310043, ACD), respectively. *Thra1* mRNA was analyzed at embryonic day (E) 10.5, E14.5, E16.5, and 18.5 and postnatal day (P) 3, P7, P14, and P56. All mice were anesthetized with 3% pentobarbital sodium (2 mL/kg) and fixed by cardiac perfusion with PBS followed by 10% neutral buffered formalin before decapitation. Formalin-perfused, fixed mouse embryo (E10.5 and E14.5) and brain (E16.5, E18.5, P3, P7, P14, and P56) were dehydrated in gradient ethanol, transparent in xylene, embedded in paraffin and cut at a setting of 5 μm in the sagittal plane. The procedure for RNAscope hybridization was performed with an RNAscope® 2.5 HD Detection Kit (#322300, ACD) (12). The RNAscope is a DAB staining. All sections were observed with a light microscope (BX53, Olympus), and images were captured with software (CellSens Standard 3.2, Olympus).

Nissl staining

For Nissl staining experiments, male WT and male mutant mice at P0, P7, and P21 were used. The brain and sliced sections were processed as described in the manufacturer's

https://etj.bioscientifica.com
https://doi.org/10.1530/ETJ-21-0097

instructions for performing RNAscope hybridization. But all the brain tissues in this part were cut at a setting of 5 μm in the coronal plane. Nissl staining of brain slices was performed with 1% toluidine blue (Sigma-Aldrich Co.), an aniline dye that preferentially stains RNA and DNA, according to the standard procedure. All the sections were observed by the light microscope (BX53, Olympus) and the images were captured with a software (CellSens Standard 3.2, Olympus).

Electrophysiology

f-EPSPs of the mice were measured with the MED64 planar microelectrode matrix recording system (Alpha Med Science, Osaka, Japan). Acute hippocampal slices prepared for electrophysiological recordings were obtained from 3-week-old homozygous mutant and WT littermates that had been anesthetized with isoflurane and decapitated.

The fresh brain tissue was cut into 300-μm thick slices, removed, and placed into an oxygenated artificial cerebrospinal fluid containing 7.25 g/L NaCl, 0.22 g/L KCl, 2.18 g/L $NaHCO_3$, 0.12 g/L $MgSO_4$, 0.17 g/L KH_2PO_4, 1.8 g/L glucose, and 0.22 g/L $CaCl_2$ (pH 7.35–7.45). The basic stimulus was set to induce 30% of the f-EPSP maximum, and a stable 30-min baseline was recorded. LTP was provoked by high-frequency stimulation (HFS) that elicited 50% of the maximal response. We stimulated the tissue twice with HFS at 10 s interval. Recordings were made at baseline intensity for an additional hour after LTP induction. f-EPSP amplitude and slope ratios were analyzed as the LTP quantification.

Animal behaviour

Morris water maze test (MWM)

MWM is a widely used behavioral procedure for the assessment of spatial learning and memory in small rodents. The MWM test apparatus consists of a 110 cm-diameter-wide black circular pool filled with opaque tap water maintained at 22°C with added non-toxic white dye. A circular hidden escape platform (10 cm in diameter) just beneath the surface was placed within the pool surrounded by four elevated visual navigation cues (colored geometric images) above each pool quadrant to provide spatial orientation (Shanghai XinRuan Information Technology Co., Ltd). The experiment was carried out according to the procedure of the mouse water maze experiment (13). EnthoVision XT Animal Trajectory Tracking System (Noldus, Netherlands) was used to determine the escape latency to find the platform (MWM training) and times of crossing of target quadrant and platform area in the spatial probe trial (MWM testing).

Elevated zero maze test

Anxiety-like behavior was measured using the elevated zero maze (EZM) (Shanghai XinRuan Information Technology Co., Ltd). It was a ring-shaped apparatus, elevated 40 cm from the floor, consisted with a circular platform (outer diameter 45 cm, width 5 cm). The circular platform was divided into four quadrants of equal lengths with two open arms (with a 0.5-cm-high curb to prevent falls) and two equal closed arms (surrounded by an 11-cm wall from the surface of the maze). Each mouse was placed in one closed arm of the maze facing one of the open arms, and 5 min of free exploration was recorded by the EnthoVision XT Animal Trajectory Tracking System (Noldus, Netherlands). The following events: the total distance of traveling, the percentage of time spent in the open arms, the number of entries into the open arms (an open arm entry is defined as the mouse's four paws in an open arm), the latency to visit the open arms (the time of the mouse's first visit to an open arm), the percentage of freezing time (the freezing time was defined as the mouse not moving or immobility), the number of rearing (rising on the hind paws) in the closed arms, and the number of head dipping (scanning over the side of the maze) in the open arms.

RNA sequencing

The gene expression profiling by RNA-seq and qPCR were performed in the hippocampus of four 3-week-old homozygous mutant mice and four WT control littermates. Total RNA was extracted following the standard RNAiso Plus protocol (Takara Bio, Japan), then qualified and quantified using the Agilent 2100 Bioanalyzer (Thermo Fisher Scientific). The first step in the workflow involves purifying mRNA molecules from total RNA using oligo(dT)-attached magnetic beads. Following purification, mRNA was fragmented into small pieces using a fragmentation reagent. First-strand cDNA was generated using random hexamer-primed RT, then was followed by second-strand cDNA synthesis. The synthesized cDNA was subjected to end-repair and then was 3' adenylated. Adaptors were ligated to the ends of these 3' adenylated cDNA fragments. The products are then purified and enriched with PCR amplification. We then quantified the PCR yield by Qubit and pooled samples together to make a single strand DNA circle (ssDNA circle), which gave the final library. DNA nanoballs (DNBs) were generated with the ssDNA circle by rolling circle replication (RCR) to enlarge the fluorescent signals at the sequencing process. The DNBs were loaded into the patterned nanoarrays and single-

https://etj.bioscientifica.com
https://doi.org/10.1530/ETJ-21-0097

end read of 50 bp were read through on the BGISEQ-500 platform (BGI, Shenzhen, China) (14).

Identification and functional annotation of the DEGs

Reads from each sample were aligned to the mouse genome (GRCm38) using HISAT2 (15). We detected DEGs with DEGseq following the manufacturer's instructions (16). Fold-change ≥ 2 and adjusted *P* value ≤ 0.001 were set as the significance thresholds. Gene ontology (GO) analysis and Kyoto Encyclopedia of Genes and Genomes (KEGG) enrichment analysis of DEGs were both performed using pHYPER, a function in R. A false discovery rate (FDR) no greater than 0.05 was defined as significantly enriched.

Validation of the RNA-seq results by qPCR

RNA was reverse transcribed into cDNA using PrimeScript™ RT Master Mix (RR036A, Takara Bio). Two-step quantitative real-time PCR (qPCR) was performed in triplicate using an oligo-dT RT primer and SYBR Premix Ex Taq II (RR820A, Takara Bio) with a Light Cycler 480 (Roche). The results were calculated using the comparative Ct method formula, 2−ΔΔCt, and the results were normalized against the expression of the housekeeping gene *Gapdh*. Statistical significance was calculated by *t* test using GraphPad Prism 8 software.

Results

Spatial and temporal expression of *Thra1* mRNA in the mouse hippocampus

We analyzed *Thra1* mRNA expression levels in the mouse hippocampus by RNAscope at E10.5, E14.5, E16.5, E18.5, P3, P7, P14, and P56. Validation of the RNAscope method was performed using negative and positive control probes (shown in Supplementary Fig. 1, see section on supplementary materials given at the end of this article). *Thra1* mRNA was detected as early as E10.5 in the neuroepithelium of cerebral vesicles (shown in Fig. 1A; a and b). With the development of the hippocampus, *Thra1* mRNA was observed in the hippocampal primordium at E14.5 (shown in Fig. 1A; c and d) and in the newly developed Ammon's horn of the hippocampus at E16.5 (shown in Fig. 1A; e and f). From E16.5 to P14, *Thra1* mRNA was expressed in all the layers of the Ammon's horn in the hippocampus (shown in Fig. 1A; f, h and 1B; A2, A3, A4, A5, B2, B3, B4, B5, C2, C3, C4, and C5), but decreased at P56 (shown in Fig. 1B; D2, D3, D4, and D5).

The development of the DG areas of the hippocampus occurred later than that of Ammon's horn of the hippocampus, which includes the outer arm and the inner arm. *Thra1* mRNA was expressed in the outer arm of DG areas as early as E18.5 (shown in Fig. 1A; i). From P3 to P14, *Thra1* mRNAs were expressed in all layers of the DG areas (shown in Fig. 1B; A6, A7, A8, B6, B7, B8, C6, C7, and C8), but slightly decreased at P56 (shown in Fig. 1B; D6, D7, and D8).

Histological alterations in the hippocampus

The cytoarchitecture of the hippocampus were shown in Fig. 2A, at P0 (A–C), P7 (D–F), and P21 (G–I). Fig. 2 (A3-I3 and A4-I4) shows the cytoarchitecture of the DG and CA1 areas of the hippocampus, respectively, which correspond to the yellow box area in A1-I1.

In the CA1 area, at P0, the neurons migrated from the ventricular zone to the CA1 area in the $Thra^{+/+}$ mice (shown in Fig. 2A; A4), whereas a large number of neurons accumulated in the ventricular zone in the mutant ($Thra^{E403X/+}$ and $Thra^{E403X/E403X}$) mice (shown in Fig. 2A; B4 and C4). At P7, the neurons in the $Thra^{+/+}$ mice had completed migration, and the borders between the sp, sr, and slm were clear (shown in Fig. 2A; D4). Compared with those of the $Thra^{+/+}$ mice, the neurons migrated from the ventricular zone to the stratum pyramidale of CA1 area in the mutant ($Thra^{E403X/+}$ and $Thra^{E403X/E403X}$) mice, in a manner similar to that of the $Thra^{+/+}$ mice at P0, indicating that *Thra* mutation results in delayed migration of neurons in CA1. The borders between the four layers were indistinguishable in the $Thra^{E403X/E403X}$ mutant mice (shown in Fig. 2A; F4), whereas the boundaries of each layer in the $Thra^{E403X/+}$ mice was clear, although there were still more cells in the stratum oriens that have not migrated to the stratum pyramidale of CA1 area (shown in Fig. 2A; E4). At P21, the neurons in the $Thra^{+/+}$ mice were arranged in order (shown in Fig. 2A; G4), whereas the arrangement of the neurons was loose and disorganized in the $Thra^{E403X/E403X}$ mice (shown in Fig. 2A; I4). The thickness of the stratum oriens was higher in the $Thra^{+/+}$ mice than in the $Thra^{E403X/+}$ mice and $Thra^{E403X/E403X}$ mice (shown in Fig. 2B; a). The total thickness of the CA1 region was thinner in the mutant ($Thra^{E403X/+}$ and $Thra^{E403X/E403X}$) mice than $Thra^{+/+}$ mice (shown in Fig. 2B; c). The cell numbers in the pyramidal cell layer of CA1 area in the $Thra^{E403X/E403X}$ mice were less than those in the $Thra^{+/+}$ mice and $Thra^{E403X/+}$ mice (shown in Fig. 2B; d).

In the DG region, the neuronal cells in the three genotypes mice were migrating at P0 (shown in Fig. 2A;

https://etj.bioscientifica.com
https://doi.org/10.1530/ETJ-21-0097

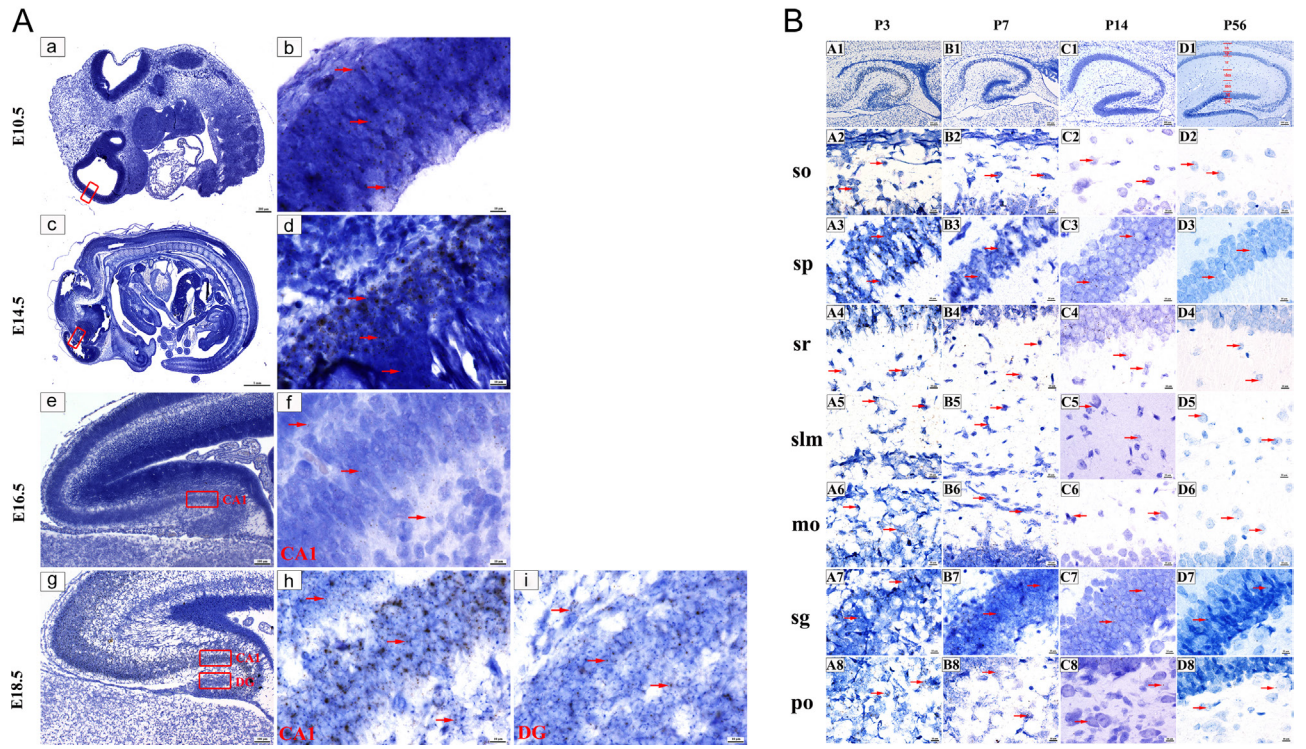

Figure 1

Spatial and temporal expression of *Thra1* mRNA in mouse hippocampus by RNAscope. (A) RNAscope hybridization demonstrates the dynamic change of *Thra1* mRNAs in mouse hippocampus during the embryonic period. Formalin-perfused, fixed mouse embryo (E10.5 and E14.5) and brain (E16.5, E18.5, P3, P7, P14, and P56) were dehydrated in gradient ethanol, transparent in xylene, embedded in paraffin, and cut at a setting of 5 μm in the sagittal plane. The cytoarchitecture of the hippocampus in b, d, f (100×) is corresponding to the red squares in the sagittal plane of brain (a, c, e, 10×), respectively. The cytoarchitecture of the hippocampus in h and i (100×) is corresponding to the red squares in the sagittal plane of brain (g, 10×), with h denoting CA1 and i denoting DG area. The red arrow shows the *Thra1* mRNA hybridized to the probes. Scale bar: 200 μm for a, 1 mm for c, 100 μm for e, g, and 10 μm for b, d, f, h, i. (B) RNAscope hybridization demonstrates the dynamic change of *Thra1* mRNAs in mouse hippocampus during the postnatal period. A1, B1, C1, and D1 show the overall structure of the hippocampus at P3, P7, P14, and P56. A2-A8, B2-B8, C2-C8, and D2-D8 show structure of the sublayers in the hippocampus at P3, P7, P14, and P56, respectively. Taking the hippocampal structure of P56 as an example, the names and boundaries of the layers of hippocampal CA and DG are marked in D1. The red arrow shows the *Thra1* mRNA hybridized to the probes. E, embryonic day; P, postnatal day; CA1, cornu ammonis area 1; DG, dentate gyrus; so, stratum oriens; sp, stratum pyramidale; sr, stratum radiatum; slm, stratum lacunosum moleculare; mo, moleculare layer; sg, stratum granulosum; po, polymorph layer.

A3, B3, and C3), and no significant differences were found. At P7, the neurons in the *Thra*$^{+/+}$ and *Thra*$^{E403X/+}$ mice had finished migration, and the borders between the layers were clear (shown in Fig. 2A; D3 and E3), whereas the borders between the three layers were indistinguishable in the *Thra*$^{E403X/E403X}$ mice (shown in Fig. 2A; F3). At P21, the neurons in the *Thra*$^{+/+}$ mice were arranged in order (shown in Fig. 2A; G3), whereas the arrangement of the neurons was disorganized and dense in the *Thra*$^{E403X/E403X}$ and *Thra*$^{E403X/+}$ mice (shown in Fig. 2A; H3 and I3). The total thickness of the DG region was thinner in *Thra*$^{E403X/E403X}$ mice than *Thra*$^{+/+}$ mice (shown in Fig. 2B; c), whereas no significant difference in the thickness of each layer or the cell numbers of the granular cell layer in DG area were found between the WT and the *Thra*^{E403X} mutant mice at P21 (shown in Fig. 2B; b and d).

Impaired LTP in the hippocampus

Spatial learning and memory require synaptic transmission, which is characterized as the LTP of f-EPSPs. We examined LTP in acute hippocampal slices of juvenile mice at P21. The LTP results were evaluated by measuring baseline f-EPSP% after HFS. The percentage of the f-EPSP slope and f-EPSP amplitude in the *Thra*$^{E403X/E403X}$ group was significantly lower than that in the *Thra*$^{+/+}$ group (shown in Fig. 3, $P < 0.05$). The impairment was 60.9% in the fEPSP slope and 49.7% in the fEPSP amplitude.

Behavioral abnormalities

In contrast to the *Thra*$^{+/+}$ mice, the time of escape latency to find the platform in the *Thra*$^{E403X/+}$ mice was longer than

https://etj.bioscientifica.com
https://doi.org/10.1530/ETJ-21-0097

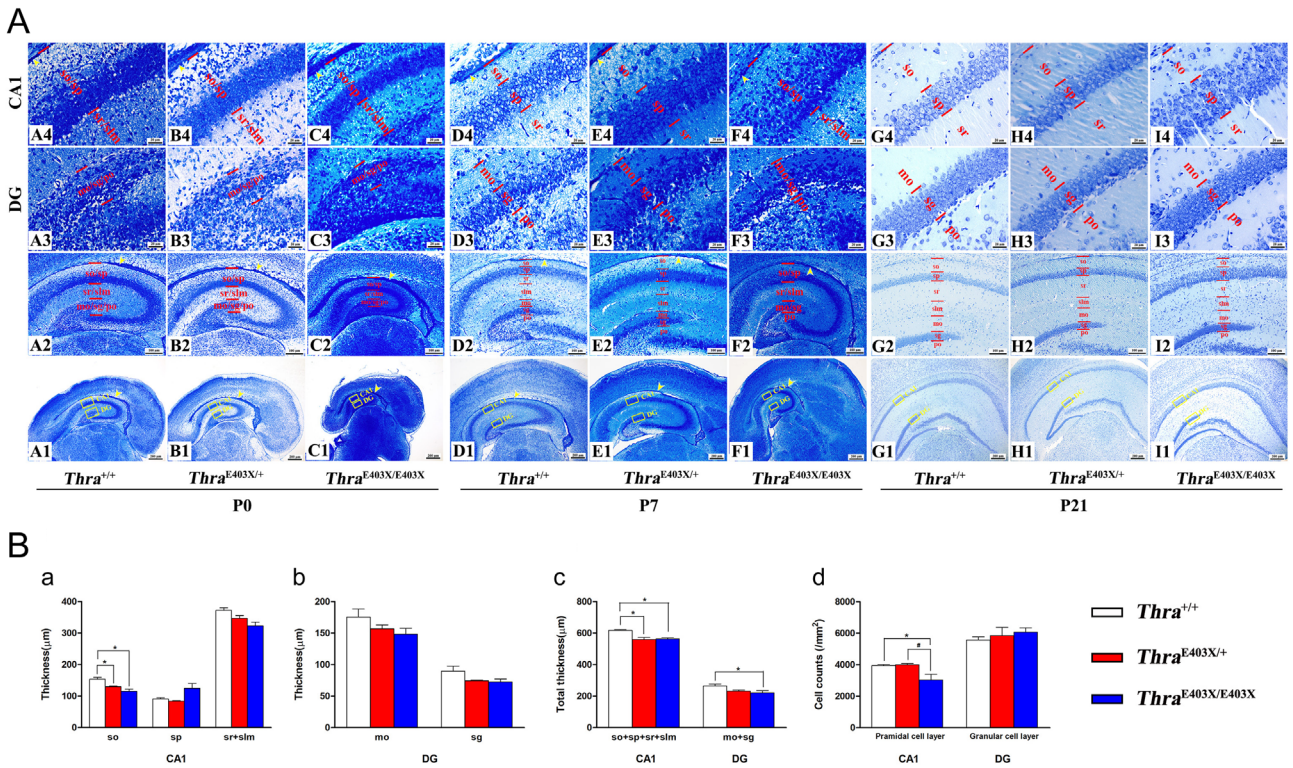

Figure 2

Representative photomicrographs of Nissl-stained coronal sections of the hippocampus. (A) The cytoarchitecture of the hippocampus (A1-I1, 4×; A2-I2, 10×) at postnatal day (P) 0 (A–C), P7 (D–F), and P21 (G–I). A3-I3 and A4-I4 showing the cytoarchitecture of the DG and CA1 area of hippocampus, respectively, which is corresponding to the yellow rectangle area in A1-I1. The yellow arrow denotes subventricular zone. Scale bar: 200 μm for A1-I1; 100 μm for A2-I2; and 20 μm for A3-I3 and A4-I4. All the brain tissues were cut at a setting of 5 μm in the coronal plane, and n = 3 for each genotype male mice at P0, P7, and P21, respectively. (B) Quantitation of the hippocampal sublayer thickness and the cell numbers in the pyramidal cell layer of the CA1 and granular cell layer in the DG at postnatal day 21. The maximal coronal section at the hippocampal level (corresponding to −2.92 mm from Bregma in adult mice (Paxinos brain atlas)) was used to analyze the morphology of hippocampus. The measurement of the layer thickness and the cell number were performed in the region where the highest point of the outer arm of the DG area, and the corresponding CA1 area. Two slides of each mouse were selected for the measurement and cell count of each sublayer in the CA1 or DG region of the hippocampus, average as the final result of each mouse. Three male mice were used for this experiment for each genotype. The number of cells in CA1 pyramidal cell layer and DG granule cell layer were corrected for the area of the counting region: cell counts/mm^2 at 40× objective. Data were presented as the mean ± S.E.M. Statistical analysis was calculated by one-way ANOVA. *Compared with *Thra*$^{+/+}$, $P < 0.05$; #Compared with *Thra*$^{E403X/+}$, $P < 0.05$.

that in the *Thra*$^{+/+}$ mice during the period of training (Fig. 4A; a). After 4 days of training, when the platform was removed, the times of crossing both the target quadrant and the platform area were also reduced in the *Thra*$^{E403X/+}$ mice than in the *Thra*$^{+/+}$ mice (Fig. 4A; b).

Mice naturally prefer the enclosed spaces, which makes them feel safe, but the anxious mice spend more time in the enclosed arms. The Elevated zero maze test showed that the total distance of traveling during the 5 min trial was shorter and the time of latency to visit the open arms was longer in the *Thra*$^{E403X/+}$ mice than in the *Thra*$^{+/+}$ mice (Fig. 4B; a and b). The time percentage of both the immobility and not moving were higher in the *Thra*$^{E403X/+}$ mice than in the *Thra*$^{+/+}$ mice (Fig. 4B; c). Moreover, the number of either entries into the open arms or the head dipping in the open arms was less in the *Thra*$^{E403X/+}$ mice than in the *Thra*$^{+/+}$ mice (Fig. 4B; d and f. Although the *Thra*$^{E403X/+}$ mice spent less time in the open arms and had less numbers of the rearing behavior in the closed areas, no significant difference was found between the WT and mutant mice (Fig. 4B; e and f).

Transcriptome changes

An average of approximately 24.11 M reads per sample were generated. The average mapping ratio with the reference genome was 95.9%, and the average mapping ratio with genes was 77.78%. A total of 17,994 genes were detected. The raw NGS data were submitted to the National Center for Biotechnology Information (NCBI) Sequence Read Archive (SRA). The SRA accession number is PRJNA727394. A comparison of hippocampal gene

https://etj.bioscientifica.com
https://doi.org/10.1530/ETJ-21-0097

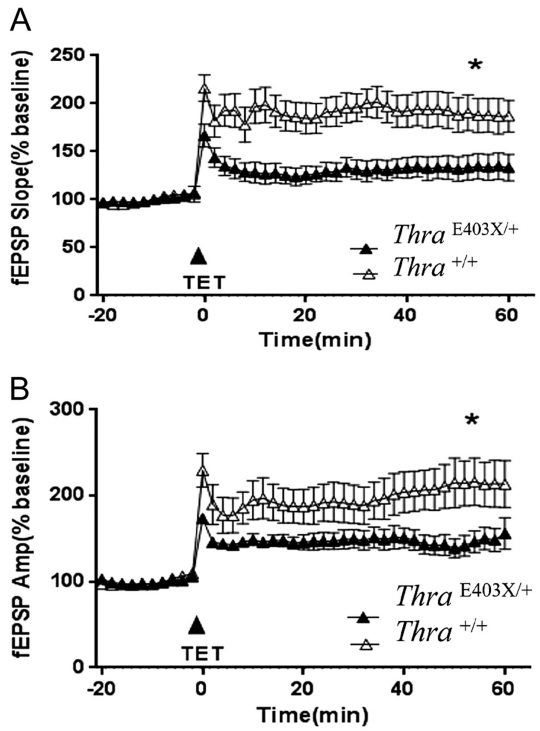

Figure 3
Impaired long-term potentiation. Long-term potentiation (LTP) was performed in the male *Thra*$^{E403X/E403X}$ mice (n = 7) and male WT mice (n = 5) at postnatal day 21. LTP was induced by HFS, measured as an increase in f-EPSP slope and amplitude, expressed as a percentage of the baseline of the f-EPSP slope and amplitude after HFS in mice. f-EPSP slope and amplitude were reduced in the *Thra*$^{E403X/E403X}$ group. Data are expressed as the mean ± S.E.M. *Compared with the *Thra*$^{+/+}$, $P < 0.05$. Statistical analysis was calculated by the Student's t test. f-EPSP, feld excitatory postsynaptic potential; HFS, high-frequency stimulation; TET, tetanic high-frequency stimulation.

expression between homozygous mutant mice and WT mice led to the identification of 754 DEGs, including 361 upregulated genes and 393 downregulated genes (shown in Fig. 5A). Predictably, a hierarchical clustering heat map based on these DEGs revealed relatively distinct separation between the homozygous mutant and WT mice (shown in Fig. 5B).

GO and KEGG pathway analyses

The DEGs were subjected to GO analysis and KEGG pathway enrichment analysis to understand the gene biological functions. Notably, metabolic process, developmental process, immune system process within the biological process category, such as synapse within the cellular component category, binding, nucleic acid binding transcription factor activity, transcription factor activity, and protein binding within the molecular function category were the enriched GO terms. In particular, ion channel-related genes are enriched for 'membrane' GO term. Pathways including the PI3K-Akt signaling pathway, ECM–receptor interaction, and neuroactive ligand–receptor interaction were found to be enriched pathway terms. Several immune-associated pathways, such as complement and coagulation cascades, the NF-kappa B signaling pathway, the cytokine-cytokine receptor interaction pathway, and primary immunodeficiency, were also represented (shown in Fig. 5C and D).

qPCR analysis of gene expression

To verify the results of the RNA-seq analyses, genes reported to be regulated by T3, genes associated with neurodevelopment, and genes that enriched for GO terms or KEGG pathways were selected for qPCR analysis. Validation by qPCR analyses revealed that 25 genes were significantly dysregulated in *Thra*^{E403X} homozygous mutant mice compared to WT mice (shown in Fig. 6, $P < 0.05$). For example, *Itga7, Kdr*, and *Il2rb* for PI3K-Akt signaling pathway. *Col6a1, Gp1ba, Itga10, Itga11,* and *Spink10* for ECM–receptor interaction. *C3, Ccl17, Cxcl5,* and *Ciita* for immune- and inflammatory-associated pathways. The qPCR results showed changes similar to those identified through the gene expression analyses.

Discussion

In this study, we investigated the spatial and temporal expression of *Thra1* mRNA continuously in the embryonic and the postnatal hippocampus of mice using an ultrasensitive *in situ* hybridization method (RNAscope). *Thra1* mRNA was highly expressed during the period from the emergence of the cerebral vesicle neuroepithelium to the development of the hippocampus, and the expression was slightly decreased in adulthood, which indicates *TRα1* is important not only for the developing hippocampus but also for the adult hippocampus. The previous study by Wallis *et al* used a mouse strain that expresses TRα1-GFP protein allowing examination of TRα1 expression in the brain. Their results showed that TRα1 was expressed in the stratum pyramidale and in the granular cell layer and hilar region of the dentate gyrus, as well as scattered in the stratum oriens and the stratum radiatum in the adult hippocampus (17), which is consistent with our results. Both her and our study found TRα1 was expressed in subgranular zone (SGZ), where the neural stem cells originated from. It indicated that TRα1 would play an important role in the regeneration of adult dentate gyrus.

https://etj.bioscientifica.com
https://doi.org/10.1530/ETJ-21-0097

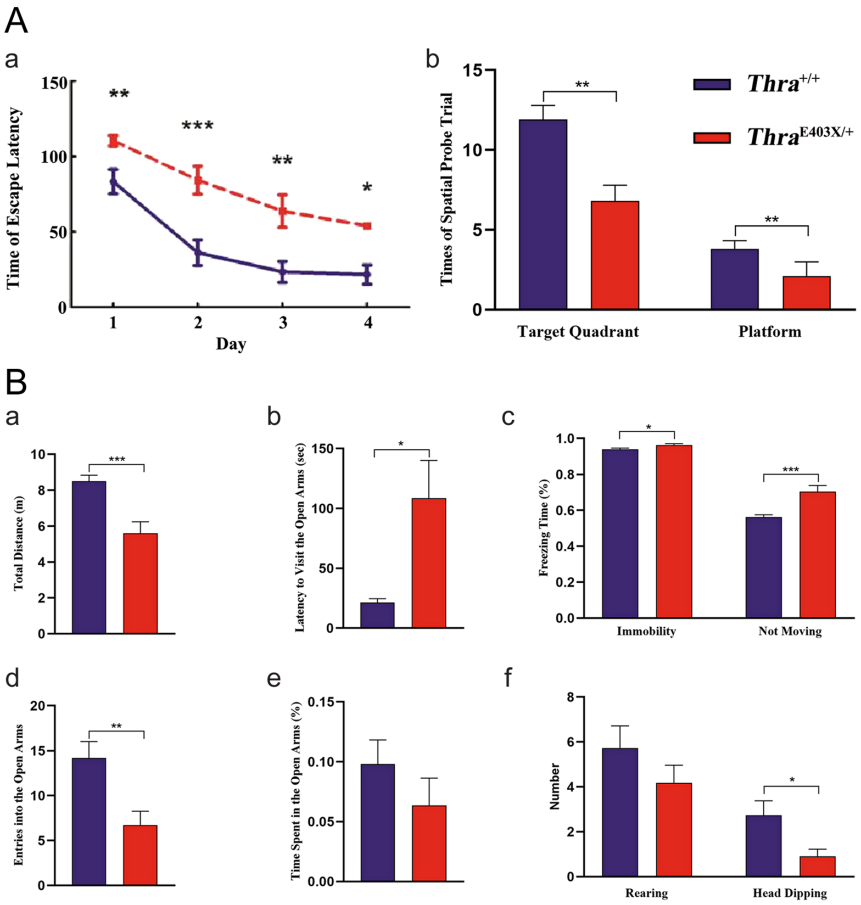

Figure 4
Behavioral abnormalities of hippocampal origin. (A) Learning and memory performance in Morris Water Maze test. Morris water maze (MWM) test was performed in the *Thra*$^{E403X/+}$ mice and *Thra*$^{+/+}$ mice at 16 weeks. n = 11 for male *Thra*$^{E403X/+}$ mice and male *Thra*$^{+/+}$ mice, respectively. (A) (a) Time of escape latency. (b) Times of crossing of target quadrant and platform area in the spatial probe trial. Data are presented as mean ± S.E.M..Statistical analysis was calculated by the Student's t test. Compared with the *Thra*$^{+/+}$ mice: *P < 0.05; **P < 0.01; ***P < 0.001. (B) Anxiety-like behavior in Elevated zero maze test. Elevated Zero Maze Test was performed in the *Thra*$^{E403X/+}$ mice and *Thra*$^{+/+}$ mice at 16 weeks. n =11 for male *Thra* $^{E403X/+}$ mice and male *Thra*$^{+/+}$ mice, respectively. (B) (a) Total distance of traveling. (b) Latency to visit the open arms. (c) Percentage of freezing time. (d) Number of entries into the open arms. (e) Percentage of time spent in the open arms. (f) Number of rearing and head dipping events. Data are expressed as the mean ± S.E.M. Statistical analysis was calculated by the Student's t test. Compared with the *Thra*$^{+/+}$ mice: *P < 0.05; **P < 0.01; ***P < 0.001.

Thyroid hormones have been implicated in multiple processes related to brain formation in mammals, such as neuronal progenitor proliferation, neuronal migration, and neural maturation (18). Thyroid hormone deficiency results in cell death (reduction in cell number) in the hippocampus and that the volume of the CA1 pyramidal cell layer is significantly smaller in hypothyroid groups than in the control groups (19, 20). Consistent with the previous studies, the present study also showed that *Thra*^{E403X} mutation results in the obvious cytoarchitectual differences. First, *Thra*^{E403X} mutation results in the severely delayed migration of neurons in both CA1 and DG areas at P0 and P7. Second, at P21, *Thra*^{E403X} mutation results in the thinner total thickness of both CA1 and DG region, as well as less cells in pyramidal cell layer of CA1 area. Third, at P21, *Thra*$^{E403X/E403X}$ mutation results in the disordered neuronal distribution in the hippocampus.

Thra$^{E403X/+}$ heterozygous mice faithfully recapitulate clinical features of human RTHα, such as delayed postnatal growth and development, neurological and motor coordination deficits, and anemia (11). In the present study, we evaluated the hippocampal behavior in the 16-week-old heterozygous mutant mice, including the Morris water maze test related to learning and memory and the Elevated zero maze test related to emotion regulation. The heterozygous mutant mice showed the impaired learning and memory, as well as anxiety. Since the *Thra*$^{E403X/E403X}$ mice die before 30 days of age, and usually the behavioral experiments are used for the adult mice, we selected LTP to evaluate the learning and memory of the 3-week-old *Thra*$^{E403X/E403X}$ mice. Our study showed that the *Thra*$^{E403X/E403X}$ mutation results in the impaired LTP in the hippocampus, which is similar to those showing hypothyroidism-induced plasticity impairment (21). Our results suggested that the impaired LTP seen in hypothyroid brains would be mediated by unliganded TRα1. The *Thra*^{E403X} mouse model might be useful for studying the deficits of learning and memory, as well as anxiety in RTHα.

The hippocampal transcriptomic alterations caused by *Thra*$^{E403X/E403X}$ mutation pointed to some KEGG and GO pathways were enriched, such as PI3K-Akt signaling, ECM–receptor interaction, neuroactive ligand–receptor interaction, immunology and inflammation, and membrane ion channel.

https://etj.bioscientifica.com
https://doi.org/10.1530/ETJ-21-0097

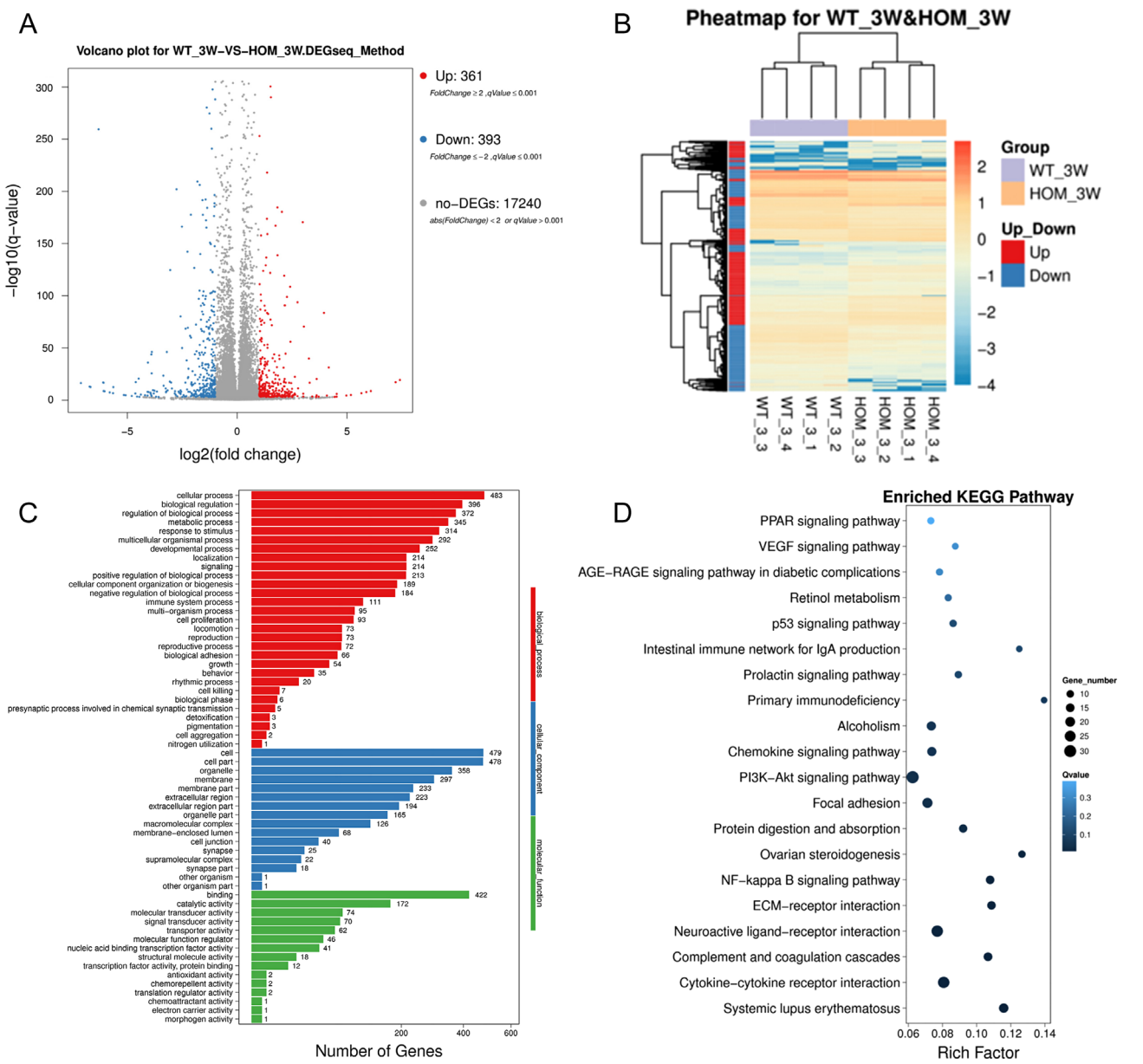

Figure 5

Transcriptomic changes induced by *Thra*^{E403X}. (A) Volcano plot for differentially expressed gene mRNAs. (B) Hierarchical clustering analysis for differentially expressed gene mRNAs. Pheatmap is the abbreviation of pretty heatmap (a function of R). (C) Gene ontology analysis for differentially expressed gene mRNAs. (D) KEGG pathway analysis for differentially expressed gene mRNAs. The lower q-value indicates the more significant enrichment. Point size indicates DEG number (The bigger the ball, the more numbers the detected genes). Rich Factor refers to the value of enrichment factor, which is the quotient of foreground value (the number of DEGs) and background value (total gene amount). The larger the value, the more significant enrichment. Eight samples were codified as follows: HOM_3W, hippocampus sample from male *Thra*$^{E403X/E403X}$ mice at 3-week-old (n = 4); WT_3 W, hippocampus sample from male *Thra*$^{+/+}$ mice at 3-week-old (n = 4).

PI3K-Akt pathway

The PI3K-Akt signaling pathway plays a significant role in neuronal health, by affecting synapse formation and maintenance, and contributes to LTP and synaptic plasticity (22, 23). Several rapid physiological effects of thyroid hormone on mammalian cells *in vitro* have been shown to be mediated by phosphatidylinositol 3-kinase (PI3K). Importantly, mutant TRβ was previously shown to activate PI3K via protein–protein interactions in TRβ$^{PV/PV}$ mice

https://etj.bioscientifica.com
https://doi.org/10.1530/ETJ-21-0097

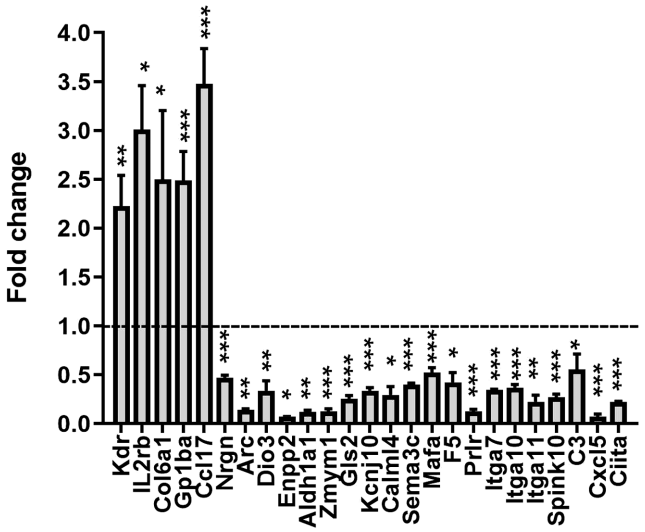

Figure 6
Validation by qPCR analyses. Relative mRNA levels of 25 DEGs were evaluated in *Thra*$^{+/+}$(n = 4) and *Thra* $^{E403X/ E403X}$ mice (n = 4). The results were calculated using the comparative Ct method formula 2−ΔΔCt method and normalized against the housekeeping gene Gapdh. Data were presented as the mean ± s.e.m. *Thra*$^{+/+}$ control was set to 1. Statistical analysis was calculated by the Student's t test. *P < 0.05; **P < 0.01; ***P < 0.001.

(24). Whether mutant TRα1 can activate PI3K via protein-protein interaction, which deserves further investigation.

ECM and neuroactive ligand–receptor interaction pathway

ECM proteins and receptors play vital roles as guidance molecules during CNS development and have been implicated in the maintenance of stable neuronal connections and in the regulation of synaptic plasticity (25, 26). The involvement of ECM proteins would explain the impaired LTP of *Thra*$^{E403X/E403X}$ mice in the present study.

Immune- and inflammatory-associated pathway

Interestingly, many immune and inflammatory genes have been found to be differentially expressed in the *Thra*$^{E403X/E403X}$ mice. These DEGs, including *C3, C8b, Ccl17, Cd4, Cd40, Gata3*, and *Cxcl5*, were found to be enriched in a number of immune-related pathways. Neuroinflammation has been reported to be associated with the abnormal brain development (27, 28, 29, 30). Our study indicated that immune and inflammatory pathway would be involved in RTHα-associated neurological diseases.

Membrane ion channel pathway

Ion channels are ubiquitous across several cell types, including progenitor cells, migrating neurons, and differentiated neurons. The precise control of ionic flux (calcium, sodium, and potassium) contributes to the developmental processes such as neural proliferation, migration, and differentiation (31). The previous studies revealed that thyroid hormone regulates dopaminergic neuron development from ventral midbrain neural stem cells by modulating TRPC1-mediated calcium signaling (32). In the present study, some ion channel-related genes were enriched for 'membrane' in Gene Ontology, which included *Trpm5, Catsperg2, Asic4, Htr3a, Gabrq, Glra2, Kcnk1, Ano3, Pkd2l1, Cntn2, Trpv4, Kcnj10, and Kcne2*. The membrane ion channel hypotheses would be a new direction for further work on the pathogenesis of RTHα.

The DEGs identified in the present study cover a wide range of physiological and biochemical processes, indicating the complicated effects of TRα1 action in the brain. Calml4 protects against spatial learning impairment in a mouse model of Alzheimer's disease (33). Enpp2 affects cell adhesion and cell positioning in neuronal progenitors located in the ventricular zone of the cerebral cortex (34). Enpp2-knockout mice display neural tube defects and neurite outgrowth deficits (35). Arc is critical for long-term potentiation and depression of synaptic transmission, homeostatic synaptic scaling, and adaptive functions such as long-term memory formation (36). Previous studies have demonstrated that *Nrgn* (RC3), a direct target of T3, participates in postsynaptic events such as those affecting LTP (19, 37). Prolactin (PRL) acts through its membrane receptor, which is widely distributed throughout the body (38). This hormone was previously thought to be involved solely in female reproduction. However, it can also regulate neurogenesis in both the subventricular zone (SVZ) and the hippocampus (39). Moreover, PRL may exert neuroprotective effects in the hippocampus of adult animals exposed to chronic stress or subjected to hippocampal infusion of kainic acid (39). In this study, genes involved in different aspects of metabolism were also identified, such as *Aldh1a1* (retinol metabolism) and *Gls2* (glutamine metabolism). The determination of the mechanism that connect these genes and TRs requires further experiments. The mRNA levels of *Nrgn, Dio3*, and *Sema3c* were significantly decreased in *Thra*$^{E403X/ E403X}$ mice, which was consistent with previously reported evidence indicating that they are T3-regulated genes (40, 41, 42). Recently, it was reported that both thyroid hormone

deficiency and unliganded TRα1 caused a decrease in the number of parvalbumin (PV)-expressing neurons, as a subpopulation of gamma-aminobutyric acid (GABA) interneurons, in the cortex and hippocampus (43, 44, 45, 46). In agreement with their results, our RNA-seq data showed that some genes, such as *Flywch2, Pvalb,* and *Syt2,* which are preferentially expressed in PV+neurons were downregulated in *Thra*$^{E403X/E403X}$ mice compared with WT mice. The results from mice with both thyroid hormone deficiency and unliganded TRα1 mutation suggested that GABAergic neurons would be the direct targets of TH/TRα1 during brain development.

In summary, the *Thra* ^{E403X} mutation results in histological and functional abnormalities, as well as dysregulated genes in the mouse hippocampus. This study on the *Thra* ^{E403X} mutation offers new insights into the potential biological causes of RTHα-associated neurological diseases.

Supplementary materials

This is linked to the online version of the paper at https://doi.org/10.1530/ETJ-21-0097.

Declaration of interest

Weiping Teng is an Editorial Board Member of the European Thyroid Journal. He was not involved in the editorial or review process of this paper, on which he is a listed authors. The other authors declare that they have no other competing or financial interests.

Funding

This study was supported by Chinese National Natural Science Foundation Grants 81970681 and 81570711 to Xiaochun Teng.

Author contribution statement

XiaochunTeng, Zhongyan Shan, and Weiping Teng designed and supervised the study. Pingping Dang performed the RNAscope, Nissl staining, Elevated zero maze test, and prepared the hippocampus samples for RNA-seq. Yingxin Fang wrote the manuscript, analyzed the RNA-seq data, and performed the qPCR. Ranran Wang measured the long-term potentiation. Yue Liang performed the Morris water maze test. Yue Liang, Defa Zhao, Yue Xi, Dan Zhang, and Wei Wang were responsible for mice feeding, breeding, and gene identification. XiaochunTeng revised the manuscript. All authors discussed the data and edited the manuscript.

References

1 Mullur R, Liu YY & Brent GA. Thyroid hormone regulation of metabolism. *Physiological Reviews* 2014 **94** 355–382. (https://doi.org/10.1152/physrev.00030.2013)

2 Santisteban P & Bernal J. Thyroid development and effect on the nervous system. *Reviews in Endocrine and Metabolic Disorders* 2005 **6** 217–228. (https://doi.org/10.1007/s11154-005-3053-9)

3 Liu YY & Brent GA. Thyroid hormone and the brain: mechanisms of action in development and role in protection and promotion of recovery after brain injury. *Pharmacology and Therapeutics* 2018 **186** 176–185. (https://doi.org/10.1016/j.pharmthera.2018.01.007)

4 Flamant F. Futures challenges in thyroid hormone signaling research. *Frontiers in Endocrinology* 2016 **7** 58. (https://doi.org/10.3389/fendo.2016.00058)

5 le Maire A, Bouhours-Nouet N, Soamalala J, Mirebeau-Prunier D, Paloni M, Guee L, Heron D, Mignot C, Illouz F, Joubert F, *et al.* Two novel cases of resistance to thyroid hormone due to THRA mutation. *Thyroid* 2020 **30** 1217–1221. (https://doi.org/10.1089/thy.2019.0602)

6 Bochukova E, Schoenmakers N, Agostini M, Schoenmakers E, Rajanayagam O, Keogh JM, Henning E, Reinemund J, Gevers E, Sarri M, *et al.* A mutation in the thyroid hormone receptor alpha gene. *New England Journal of Medicine* 2012 **366** 243–249. (https://doi.org/10.1056/NEJMoa1110296)

7 van Mullem AA, Chrysis D, Eythimiadou A, Chroni E, Tsatsoulis A, de Rijke YB, Visser WE, Visser TJ & Peeters RP. Clinical phenotype of a new type of thyroid hormone resistance caused by a mutation of the TRα1 receptor: consequences of LT4 treatment. *Journal of Clinical Endocrinology and Metabolism* 2013 **98** 3029–3038. (https://doi.org/10.1210/jc.2013-1050)

8 Deuker L, Bellmund JL, Navarro Schröder T & Doeller CF. An event map of memory space in the hippocampus. *eLife* 2016 **5** e16534. (https://doi.org/10.7554/eLife.16534)

9 Fries M, Bickenbach J, Henzler D, Beckers S, Dembinski R, Sellhaus B, Rossaint R & Kuhlen R. S-100 protein and neurohistopathologic changes in a porcine model of acute lung injury. *Anesthesiology* 2005 **102** 761–767. (https://doi.org/10.1097/00000542-200504000-00011)

10 Wang F, Zeng X, Zhu Y, Ning D, Liu J, Liu C, Jia X & Zhu D. Effects of thyroxine and donepezil on hippocampal acetylcholine content, acetylcholinesterase activity, synaptotagmin-1 and SNAP-25 expression in hypothyroid adult rats. *Molecular Medicine Reports* 2015 **11** 775–782. (https://doi.org/10.3892/mmr.2014.2825)

11 Liang Y, Zhao D, Wang R, Dang P, Xi Y, Zhang D, Wang W, Shan Z, Teng X & Teng W. Generation and characterization of a new resistance to thyroid hormone mouse model with thyroid hormone receptor alpha gene mutation. *Thyroid* 2021 **31** 678–691. (https://doi.org/10.1089/thy.2019.0733)

12 Wang F, Flanagan J, Su N, Wang LC, Bui S, Nielson A, Wu X, Vo HT, Ma XJ & Luo Y. RNAscope: a novel in situ RNA analysis platform for formalin-fixed, paraffin-embedded tissues. *Journal of Molecular Diagnostics* 2012 **14** 22–29. (https://doi.org/10.1016/j.jmoldx.2011.08.002)

13 Vorhees CV & Williams MT. Morris water maze: procedures for assessing spatial and related forms of learning and memory. *Nature Protocols* 2006 **1** 848–858. (https://doi.org/10.1038/nprot.2006.116)

14 Foox J, Tighe SW, Nicolet CM, Zook JM, Byrska-Bishop M, Clarke WE, Khayat MM, Mahmoud M, Laaguiby PK, Herbert ZT, *et al.* Performance assessment of DNA sequencing platforms in the ABRF Next-Generation Sequencing Study. *Nature Biotechnology* 2021 **39** 1129–1140. (https://doi.org/10.1038/s41587-021-01049-5)

15 Kim D, Langmead B & Salzberg SL. HISAT: a fast spliced aligner with low memory requirements. *Nature Methods* 2015 **12** 357–360. (https://doi.org/10.1038/nmeth.3317)

16 Wang L, Feng Z, Wang X, Wang X & Zhang X. DEGseq: an R package for identifying differentially expressed genes from RNA-seq data. *Bioinformatics* 2010 **26** 136–138. (https://doi.org/10.1093/bioinformatics/btp612)

17 Wallis K, Dudazy S, van Hogerlinden M, Nordström K, Mittag J & Vennström B. The thyroid hormone receptor alpha1 protein is expressed in embryonic postmitotic neurons and persists in most adult neurons. *Molecular Endocrinology* 2010 **24** 1904–1916. (https://doi.org/10.1210/me.2010-0175)

18 Stepien BK & Huttner WB. Transport, metabolism, and function of thyroid hormones in the developing mammalian brain. *Frontiers in Endocrinology* 2019 **10** 209. (https://doi.org/10.3389/fendo.2019.00209)

19 Koromilas C, Liapi C, Schulpis KH, Kalafatakis K, Zarros A & Tsakiris S. Structural and functional alterations in the hippocampus due to hypothyroidism. *Metabolic Brain Disease* 2010 **25** 339–354. (https://doi.org/10.1007/s11011-010-9208-8)

20 Ittermann T, Wittfeld K, Nauck M, Bülow R, Hosten N, Völzke H & Grabe HJ. High thyrotropin is associated with reduced hippocampal volume in a population-based study from Germany. *Thyroid* 2018 **28** 1434–1442. (https://doi.org/10.1089/thy.2017.0561)

21 Salazar P, Cisternas P, Codocedo JF & Inestrosa NC. Induction of hypothyroidism during early postnatal stages triggers a decrease in cognitive performance by decreasing hippocampal synaptic plasticity. *Biochimica et Biophysica Acta: Molecular Basis of Disease* 2017 **1863** 870–883. (https://doi.org/10.1016/j.bbadis.2017.01.002)

22 Gabbouj S, Ryhänen S, Marttinen M, Wittrahm R, Takalo M, Kemppainen S, Martiskainen H, Tanila H, Haapasalo A, Hiltunen M, *et al.* Altered insulin signaling in Alzheimer's disease brain – special emphasis on PI3K-Akt pathway. *Frontiers in Neuroscience* 2019 **13** 629. (https://doi.org/10.3389/fnins.2019.00629)

23 Saw G, Krishna K, Gupta N, Soong TW, Mallilankaraman K, Sajikumar S & Dheen ST. Epigenetic regulation of microglial phosphatidylinositol 3-kinase pathway involved in long-term potentiation and synaptic plasticity in rats. *Glia* 2020 **68** 656–669. (https://doi.org/10.1002/glia.23748)

24 Martin NP, Marron Fernandez de Velasco E, Mizuno F, Scappini EL, Gloss B, Erxleben C, Williams JG, Stapleton HM, Gentile S & Armstrong DL. A rapid cytoplasmic mechanism for PI3 kinase regulation by the nuclear thyroid hormone receptor, TRβ, and genetic evidence for its role in the maturation of mouse hippocampal synapses in vivo. *Endocrinology* 2014 **155** 3713–3724. (https://doi.org/10.1210/en.2013-2058)

25 Bernal J. Thyroid hormone regulated genes in cerebral cortex development. *Journal of Endocrinology* 2017 **232** R83–R97. (https://doi.org/10.1530/JOE-16-0424)

26 Lilja J & Ivaska J. Integrin activity in neuronal connectivity. *Journal of Cell Science* 2018 **131** jcs212803. (https://doi.org/10.1242/jcs.212803)

27 Montesinos MDM & Pellizas CG. Thyroid hormone action on innate immunity. *Frontiers in Endocrinology* 2019 **10** 350. (https://doi.org/10.3389/fendo.2019.00350)

28 Chavan SS, Pavlov VA & Tracey KJ. Mechanisms and therapeutic relevance of neuro-immune communication. *Immunity* 2017 **46** 927–942. (https://doi.org/10.1016/j.immuni.2017.06.008)

29 Heneka MT, McManus RM & Latz E. Inflammasome signalling in brain function and neurodegenerative disease. *Nature Reviews: Neuroscience* 2018 **19** 610–621. (https://doi.org/10.1038/s41583-018-0055-7)

30 Yirmiya R & Goshen I. Immune modulation of learning, memory, neural plasticity and neurogenesis. *Brain, Behavior, and Immunity* 2011 **25** 181–213. (https://doi.org/10.1016/j.bbi.2010.10.015)

31 Smith RS & Walsh CA. Ion channel functions in early brain development. *Trends in Neurosciences* 2020 **43** 103–114. (https://doi.org/10.1016/j.tins.2019.12.004)

32 Chen C, Ma Q, Deng P, Yang J, Yang L, Lin M, Yu Z & Zhou Z. Critical role of TRPC1 in thyroid hormone-dependent dopaminergic neuron development. *Biochimica et Biophysica Acta: Molecular Cell Research* 2017 **1864** 1900–1912. (https://doi.org/10.1016/j.bbamcr.2017.07.019)

33 Kusakari S, Nawa M, Sudo K & Matsuoka M. Calmodulin-like skin protein protects against spatial learning impairment in a mouse model of Alzheimer disease. *Journal of Neurochemistry* 2018 **144** 218–233. (https://doi.org/10.1111/jnc.14258)

34 Greenman R, Gorelik A, Sapir T, Baumgart J, Zamor V, Segal-Salto M, Levin-Zaidman S, Aidinis V, Aoki J, Nitsch R, *et al.* Non-cell autonomous and non-catalytic activities of ATX in the developing brain. *Frontiers in Neuroscience* 2015 **9** 53. (https://doi.org/10.3389/fnins.2015.00053)

35 Fotopoulou S, Oikonomou N, Grigorieva E, Nikitopoulou I, Paparountas T, Thanassopoulou A, Zhao Z, Xu Y, Kontoyiannis DL, Remboutsika E, *et al.* ATX expression and LPA signalling are vital for the development of the nervous system. *Developmental Biology* 2010 **339** 451–464. (https://doi.org/10.1016/j.ydbio.2010.01.007)

36 Nikolaienko O, Patil S, Eriksen MS & Bramham CR. Arc protein: a flexible hub for synaptic plasticity and cognition. *Seminars in Cell and Developmental Biology* 2018 **77** 33–42. (https://doi.org/10.1016/j.semcdb.2017.09.006)

37 Martínez de Arrieta C, Morte B, Coloma A & Bernal J. The human RC3 gene homolog, NRGN contains a thyroid hormone-responsive element located in the first intron. *Endocrinology* 1999 **140** 335–343. (https://doi.org/10.1210/endo.140.1.6461)

38 Bole-Feysot C, Goffin V, Edery M, Binart N & Kelly PA. Prolactin (PRL) and its receptor: actions, signal transduction pathways and phenotypes observed in PRL receptor knockout mice. *Endocrine Reviews* 1998 **19** 225–268. (https://doi.org/10.1210/edrv.19.3.0334)

39 Torner L. Actions of prolactin in the brain: From physiological adaptations to stress and neurogenesis to psychopathology. *Frontiers in Endocrinology* 2016 **7** 25. (https://doi.org/10.3389/fendo.2016.00025)

40 Gil-Ibañez P, García-García F, Dopazo J, Bernal J & Morte B. Global transcriptome analysis of primary cerebrocortical cells: identification of genes regulated by triiodothyronine in specific cell types. *Cerebral Cortex* 2017 **27** 706–717. (https://doi.org/10.1093/cercor/bhv273)

41 Salazar P, Cisternas P, Martinez M & Inestrosa NC. Hypothyroidism and cognitive disorders during development and adulthood: implications in the central nervous system. *Molecular Neurobiology* 2019 **56** 2952–2963. (https://doi.org/10.1007/s12035-018-1270-y)

42 Lee JY & Petratos S. Thyroid hormone signaling in oligodendrocytes: from extracellular transport to intracellular signal. *Molecular Neurobiology* 2016 **53** 6568–6583. (https://doi.org/10.1007/s12035-016-0013-1)

43 Uchida K, Hasuoka K, Fuse T, Kobayashi K, Moriya T, Suzuki M, Katayama N &Itoi K. Thyroid hormone insufficiency alters the expression of psychiatric disorder-related molecules in the hypothyroid mouse brain during the early postnatal period. *Scientific Reports* 2021 **11** 6723. (https://doi.org/10.1038/s41598-021-86237-8)

44 Richard S, Guyot R, Rey-Millet M, Prieux M, Markossian S, Aubert D & Flamant F. A pivotal genetic program controlled by thyroid hormone during the maturation of GABAergic neurons. *iScience* 2020 **23** 100899. (https://doi.org/10.1016/j.isci.2020.100899)

45 Gilbert ME, Sui L, Walker MJ, Anderson W, Thomas S, Smoller SN, Schon JP, Phani S & Goodman JH. Thyroid hormone insufficiency during brain development reduces parvalbumin immunoreactivity and inhibitory function in the hippocampus. *Endocrinology* 2007 **148** 92–102. (https://doi.org/10.1210/en.2006-0164)

46 Wallis K, Sjögren M, van Hogerlinden M, Silberberg G, Fisahn A, Nordström K, Larsson L, Westerblad H, Morreale de Escobar G, Shupliakov O, *et al.* Locomotor deficiencies and aberrant development of subtype-specific GABAergic interneurons caused by an unliganded thyroid hormone receptor alpha1. *Journal of Neuroscience* 2008 **28** 1904–1915. (https://doi.org/10.1523/JNEUROSCI.5163-07.2008)

Received in final form 5 March 2022
Accepted 9 March 2022
Accepted Manuscript published online 9 March 2022